1D) and barium germanate (*13*) (Fig. 1E) structures, also consist of alternating SiO_6 octahedra and Si_3O_9 three-member rings in slightly different layered arrangements.

The $Na_4Si_2(Si_6O_{18})$ structure, with nine-member tetrahedral rings cross-linked by individual octahedra, exemplifies the complexity possible with $Si^{IV}-Si^{VI}$ frameworks (*14*) (Fig. 1F). Many other framework variants with $n/m = 3$ are also possible. One example is $Ba_2Si_2(Si_6O_{18})$, a hypothetical structure with six-member rings related to the beryl topology (*15*) (Fig. 1G). More complex structures incorporating an integral multiple of three tetrahedra in rings (that is, combinations of three- plus six-, or four- plus five-member rings) are also possible. An intriguing structural possibility, as yet unknown in silicates, is a $Si^{IV}-Si^{VI}$ framework, with individual SiO_6 octahedra cross-linking continuous $n[SiO_3]$ tetrahedral chains. A sinusoidal tetrahedral chain might be linked to form a high-density silicate structure with the $n/m = 3$ stoichiometry.

Structures with $n/m > 3$: All $Si^{IV}-Si^{VI}$ framework structures with $n/m > 3$ must have on average fewer than two exposed tetrahedral oxygens per octahedral oxygen. Thus, some tetrahedra must be bound to three tetrahedral neighbors, for example, in amphibole-type double chains (1.5 exposed oxygen atoms per Si^{IV} or in layers (one exposed oxygen atom per Si^{IV}). Indeed, in the extreme case of $m = 0$ and $n = \infty$ (SiO_2 in the coesite structure), there are no exposed oxygen atoms per Si^{IV}.

Although many framework configurations with $n/m > 3$ might be imagined, only one such structure is known. The synthesis of $(Na_{1.8}Ca_{1.1})Si(Si_5O_{14})$, a new structure with $m = 1$ and $n = 5$, does feature a silicate tetrahedral layer, but details of this structure currently defy prediction by systematic means (*16*) (Fig. 1H). As expected, tetrahedra are distributed in a continuous layer cross-linked by individual SiO_6 octahedra. Those layers, with interconnected 12-member rings, are unlike any other known structure. Furthermore, 2 out of every 14 oxygen atoms are nonbridging—a feature never observed in low-pressure Si^{IV} frameworks. The possibility of $Si^{IV}-Si^{VI}$ frameworks with nonbridging oxygen atoms greatly increases the range of stoichiometries, topologies, and crystal chemical behavior that must be considered in predicting related structures.

Recognition of this class of framework silicates points to new research opportunities. These phases provide a means to investigate the high-pressure behavior of large cations. As pressure is increased, the size and shape of large sites will change, providing a tuneable probe of cation-oxygen bonding, ion exchange, and phase stability. These studies also suggest that many related structures remain to be discovered, especially through synthesis of high-pressure phases in silicate systems containing larger cations such as Rb, Cs, Sr, and Ba. Not only do these framework structures represent possible repositories of alkali and the larger alkaline earth cations in the earth's transition zone, where mixed 4- and 6-coordinated minerals are thought to be abundant (*6*, *17*), but some of these dense framework silicates, or their room-pressure germanate and titanate isomorphs, may also provide stable long-term storage environments for Sr^{90}, Cs^{137}, Tl^{204}, and other mobile components of radioactive waste.

REFERENCES AND NOTES

1. P. J. Heaney, C. T. Prewitt, G. V. Gibbs, Eds., *Silica* (Mineralogical Society of America, Washington, DC, 1994); I. Parsons, Ed., *Feldspars and Their Reactions* (Kluwer, Boston, MA, 1994); W. A. Deer, R. A. Howie, J. Zussman, *Rock-Forming Minerals Volume 4, Framework Silicates* (Wiley, New York, 1963); F. R. Ribeiro, A. E. Rodrigues, L. D. Rollmann, C. Naccache, Eds., *Zeolites: Science and Technology. NATO ASI Series, Ser. E: Applied Sciences No. 80* (Nijhoff, the Hague, Netherlands, 1984); W. M. Meier and D. H. Olson, *Zeolites* **12**, 1 (1992).
2. R. M. Hazen and L. W. Finger, *Phase Transitions* **1**, 1 (1979).
3. M. B. Kruger and R. Jeanloz, *Science* **249**, 647 (1990).
4. J. Papp, D. Kallo, G. Schay, *J. Catal.* **23**, 168 (1971); E. J. Detrekoy, P. A. Jacobs, D. Kallo, J. B. Uytterhoeven, *ibid.* **32**, 442 (1974); H. Beyer, *Acta Chim. Acad. Sci. Hung.* **84**, 25 (1975); F. A. Mumpton, *Rev. Mineral.* **4**, 177 (1981).
5. J. M. Newsam, *Science* **231**, 1093 (1986); F. Liebau, H. Gies, R. P. Gunawardane, B. Marler, *Zeolites* **6**, 373 (1986); D. E. Akporaiye, *Z. Kristallogr.* **188**, 103 (1989); C. A. Fyfe, H. Gies, Y. Feng, G. T. Kokotailo, *Nature* **341**, 223 (1989); J. V. Smith, in *Proceedings of the Eighth International Zeolite Conference, Amsterdam*, 10 to 14 July 1989, P. A. Jacobs and R. A. Van Santen, Eds. (Elsevier, Amsterdam, 1989), pp. 29–47; G. O. Brunner and W. M. Meier, *Nature* **337**, 146 (1989); K. J. Andries, *Acta Crystallogr.* **A46**, 855 (1990).
6. L. W. Finger and R. M. Hazen, *Acta Crystallogr.* **B47**, 561 (1991).
7. J. F. Stebbins and M. Kanzaki, *Science* **251**, 294 (1991).
8. R. E. G. Pacalo, D. J. Weidner, T. Gasparik, *Geophys. Res. Lett.* **19**, 1895 (1992); R. M. Hazen, R. T. Downs, P. G. Conrad, L. W. Finger, T. Gasparik, *Phys. Chem. Miner.* **21**, 344 (1994).
9. M. E. Fleet and G. S. Henderson, *Phys. Chem. Miner.* **22**, 383 (1995).
10. N. N. Nevsky, V. V. Ilyukhin, L. I. Ivanova, N. V. Belov, *Dokl. Akad. Nauk SSSR* **245**, 110 (1979).
11. N. Kinomura, S. Kume, M. Koizumi, *Mineral. Mag.* **40**, 401 (1975); D. K. Swanson and C. T. Prewitt, *Am. Mineral.* **68**, 581 (1983).
12. L. W. Finger, R. M. Hazen, B. Fursenko, *J. Phys. Chem. Solids* **56**, 1389 (1995).
13. R. M. Hazen, R. T. Downs, L. W. Finger, T. Gasparik, B. Fursenko, *Geol. Soc. Am. Abstr. Prog.* **27**, A-166 (1994).
14. M. E. Fleet and G. S. Henderson, *Eos* **76**, F710 (1995); M. E. Fleet, *Am. Mineral.* **81**, 911 (1996).
15. R. M. Hazen, A. Y. Au, L. W. Finger, *Am. Mineral.* **71**, 977 (1986).
16. T. Gasparik, J. B. Parise, B. A. Eiban, J. A. Hriljac, *Am. Mineral.* **80**, 1269 (1995).
17. J. Ita and L. Stixrude, *J. Geophys. Res.* **97**, 6849 (1992).

18. We thank C. T. Prewitt and D. Teter for helpful reviews. Supported by grants from NSF and the Carnegie Institution of Washington.

7 February 1996; accepted 8 April 1996

Evidence for Glacial Control of Rapid Sea Level Changes in the Early Cretaceous

Heather M. Stoll and Daniel P. Schrag

Lower Cretaceous bulk carbonate from deep sea sediments records sudden inputs of strontium resulting from the exposure of continental shelves. Strontium data from an interval spanning 7 million years in the Berriasian-Valanginian imply that global sea level fluctuated about 50 meters over time scales of 200,000 to 500,000 years, which is in agreement with the Exxon sea level curve. Oxygen isotope measurements indicate that the growth of continental ice sheets caused these rapid sea level changes. If glaciation caused all the rapid sea level changes in the Cretaceous that are indicated by the Exxon curve, then an Antarctic ice sheet may have existed despite overall climatic warmth.

Sea level curves based on sequence stratigraphy (*1*) imply that the sea level rose and fell 100 m or so in less than 1 million years several times during the Cretaceous. These rapid sea level changes represent a paradox, because the Cretaceous climate has typically been thought to have been too warm for extensive accumulation of continental ice, which is the only known mechanism for driving such rapid sea level changes (*2*). One interpretation is that sequence stratigraphic data are recording apparent sea level changes caused by regional tectonic activity (*3*). However, if these sea level changes are global, either there exists some non-glacioeustatic mechanism for rapidly changing sea level or the assessment of the Cretaceous as a period of continuous climatic warmth needs reevaluation.

To test whether Cretaceous sea level changes were global, we measured Sr con-

Department of Geological and Geophysical Sciences, Princeton University, Princeton, NJ 08544–1003, USA.

centrations in deep sea carbonate sediments. The Sr concentration of seawater should be sensitive to sea level changes, because when sea level drops, Sr-rich aragonite on continental shelves is exposed and is altered to calcite (*4*, *5*). Up to 90% of the Sr in the aragonite can be released to the oceans in less than 100,000 years (*6*). Because as much as 90% of carbonate accumulation occurred on continental shelves in the Early Cretaceous, compared with only 20% in the modern ocean (*7*), the impact of shelf weathering on the Sr budget was amplified. In addition, it is likely that the residence time of Sr in seawater in the Cretaceous was at least four times less than in the modern ocean (*7*), which means that the response of the ocean to rapid changes in fluxes was also amplified. If rapid regression-transgression couplets in the Cretaceous were global, deep sea carbonate should record large increases in seawater Sr concentrations over these intervals.

We investigated a 7-million-year interval in the Berriasian-Valanginian that overlaps two large sea level falls in the Haq *et al.* sea level curve (*1*). We sampled three Deep Sea Drilling Project sites (*8*) at intervals of 25,000 to 50,000 years. These records were nearly continuous and showed high carbonate contents (>50%). We were not able to analyze specific fractions of the sediment (for example, foraminiferal tests) because microfossils were not well preserved in these Lower Cretaceous sediments. Measurement of bulk carbonate rather than foraminifera may introduce additional sources of uncertainty, because changes in the distribution of flora and fauna may affect the partitioning of Sr into the sediment record. We thus examined several sites, as it is unlikely that these effects will be identical between sites.

Because poor microfossil preservation limits the utility of high-resolution biostratigraphy in these sites, we correlated records from different sites with fluctuations in $\delta^{13}C$ by visual assessment (*9*) (Fig. 1), only minimally compressing or extending portions of the record. In using carbon isotopes, our objective was not to minimize

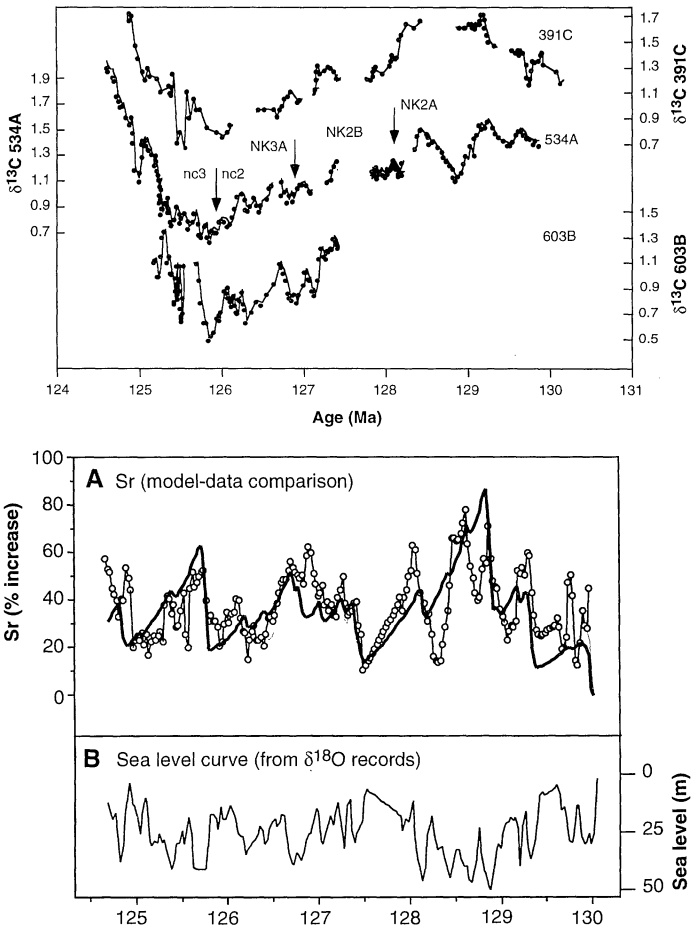

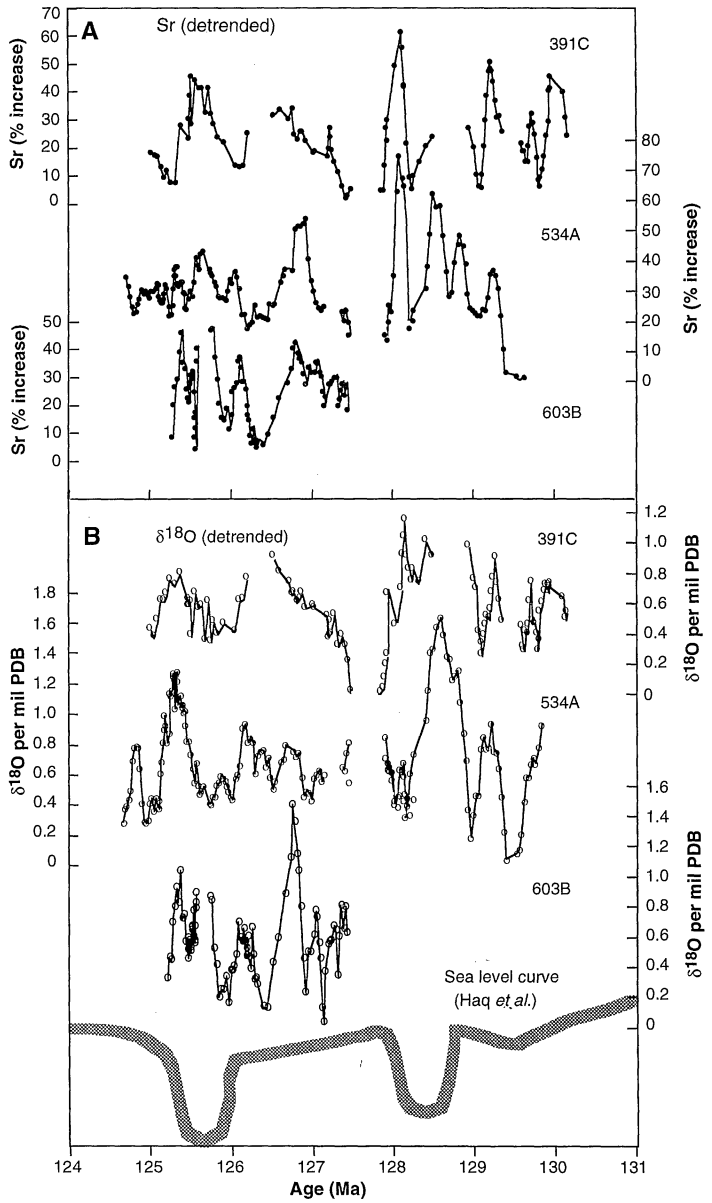

Fig. 1 (**top left**). Carbon isotope data (three-point running mean) on bulk carbonate samples from sites 391C, 534A, and 603B, plotted versus age with the use of the Haq *et al.* time scale (*1*). Labeled arrows indicate selected nannofossil data for site 534A (*10*). **Fig. 2** (**right**). (**A**) Sr concentrations (solid circles, five-point running mean) plotted versus age for sites 391C, 534A, and 603B. Sr data are normalized to 100% $CaCO_3$, detrended, and expressed as percent increases over the minimum value. (**B**) Oxygen isotope data (open circles, five-point running mean) on bulk carbonate samples plotted versus age and detrended as described in the text. Regressions in the Haq *et al.* sea level curve (*1*) are shown as a thick gray line. PDB, Pee Dee belemnite standard. **Fig. 3** (**bottom left**). (**A**) Comparison of model-calculated Sr concentrations (bold line) with the composite Sr record for sites 391C, 534A, and 603B (thin line and open circles). (**B**) Sea level curve used to force the model, based on a composite $\delta^{18}O$ record from the three sites.

offsets in the Sr and $\delta^{18}O$ records but to correlate them using an independent parameter. We estimate that the uncertainty in the correlation among sites is several hundred thousand years, which may produce apparent offsets in the Sr and $\delta^{18}O$ trends between different sites. Biostratigraphic data in site 534A (*10*) were used to apply the time scale of Haq *et al.* (*1*).

Between 128 and 124 million years ago (Ma), Sr concentrations [normalized to 100% $CaCO_3$ (*11*)] increased linearly from 400 to 800 parts per million (ppm) at all sites (*12*). This increase was likely caused by a variety of processes other than changes in sea level (for example, by a change in mid-ocean ridge hydrothermal fluxes or continental weathering rates) (*13*). To isolate the higher frequency variations of several hundred parts per million, we subtracted a linear fit to each record from the data.

The detrended Sr records exhibit high variability with sharp increases of up to 120% (*14*) over several hundred thousand years (Fig. 2A). Replicate Sr records from the carbonate fraction, obtained for two sites by removal of adsorbed Sr from noncarbonate phases with a modified cation-exchange procedure (*15*), parallel the signal in the bulk sediment with a slightly reduced amplitude. The largest excursions, which occur over 200,000 to 500,000 years, are reproduced in all records. The magnitude of the high-frequency variability implies that differential release of Sr during diagenesis was not responsible for the signal (*16*). Diagenetic Sr loss is greatest in the upper ~100 m of sediment, where pore fluid Sr can diffuse into the overlying seawater. The total amount of Sr removed from carbonate is limited by the rate of diffusion of Sr in pore fluid and cannot exceed approximately 25% (*17*). Low correlation between Sr concentrations and $CaCO_3$ content (coefficient of determination r^2 values of 0.07, 0.38, and 0.07) implies that differential Sr loss in sediments of varying carbonate content is not the primary source of Sr variability in these records. The reproducibility of the signal in multiple sites is further evidence against a diagenetic origin of the Sr signal.

Two large Sr peaks at 128 to 129 Ma and 125 to 126 Ma coincide with rapid sea level falls in the sequence stratigraphic sea level record (*1*). However, the Sr record indicates that sea level changes were more frequent and of shorter duration than indicated by the sequence stratigraphic curve, which is likely at coarser resolution (*3*).

To test whether the sea level changes were caused by continental glaciation, we compared $\delta^{18}O$ values of bulk carbonate with Sr concentrations in all three records (Fig. 2) (*18*). Previous studies have demonstrated that $\delta^{18}O$ values of bulk carbonate accurately record changes in sea surface temperature and the $\delta^{18}O$ of seawater over glacial cycles (*19*, *20*). Carbonate diagenesis may shift the mean $\delta^{18}O$ value by several per mil, making an equivocal record of absolute temperature; but high-frequency variations will be preserved, although partially attenuated (*20*, *21*). The low correlation of $\delta^{18}O$ and $CaCO_3$ content (r^2 values of 0.29, 0.32, and 0.03) suggests that differential recrystallization of sediments of varying carbonate content is not the primary source of $\delta^{18}O$ variability in these records. The reproducibility of the signal in multiple records also argues against a diagenetic origin, because diagenesis is unlikely to produce the same signal in three different sites.

The $\delta^{18}O$ records from the Early Cretaceous show high-frequency variations of 0.5 to 1.7 per mil (Fig. 2B). Periods of low temperature or high ice volume or both, recorded by increased $\delta^{18}O$ values, coincide with episodes of low sea level, which are reflected by high Sr concentrations. Large $\delta^{18}O$ peaks at 128 to 129 Ma and at 125 to 126 Ma coincide with sea level lowstands that are identified by the sea level curve (*1*). This comparison implies that periodic glaciations caused rapid sea level changes in the Early Cretaceous. It is difficult to estimate the amount of ice or sea level change directly from the $\delta^{18}O$ curves, because not only has the amplitude of the $\delta^{18}O$ variations been attenuated during diagenesis but also it is unknown how much changes in sea surface temperature contributed to changes in the $\delta^{18}O$ of the bulk carbonate.

To estimate the magnitude of the sea level change required by the data and to test whether the observed Sr signal is reasonable, we used a box model of the oceans that simulates the influx of Sr from rivers and hydrothermal circulation at mid-ocean ridges as well as the outflux of Sr due to deposition in the deep sea and in shelves of calcite and aragonite. The riverine and hydrothermal influx was set equal to average Sr removal rates calculated from shelf and deep sea carbonate accumulation rates for the Cretaceous (*7*) and was assumed to be constant. This assumption does not significantly affect model results. We used the modern coefficients for partitioning Sr between seawater and biogenic calcite and aragonite (*5*, *22*). Although some of these parameters may have varied through glacial cycles (*23*), their impact on the Sr curve is relatively minor. The higher fluxes and lower mean concentration in seawater relative to modern values yield an average residence time for Sr of 0.5 million years, which is approximately four times shorter than the modern value (*13*). The model simulated the buildup and release of Sr from shelf sediments. We assume that a 1-m thick box accumulated Sr when submerged within 50 m of the sea surface and released Sr exponentially with a time constant of 20,000 years when exposed above sea level. When the model aragonite recrystallized to calcite, 90% of Sr was released. This value corresponds to observations of Pleistocene carbonate platforms (*6*, *24*).

To simulate the frequency and relative amplitudes of sea level changes in the model, we used a composite $\delta^{18}O$ record from the three sites (*25*). Relative amplitudes obtained from the $\delta^{18}O$ record are accurate only if the relative contributions of the temperature and ice volume remain constant. In addition, averaging the record to produce a composite curve may attenuate variability because of uncertainties in correlation. However, this approach provides a reasonable first approximation for the model sea level curve. The model Sr curve reproduced much of the observed Sr variability over time scales of 200,000 to 300,000 years (Fig. 3); because of the residence time used in the calculations, the model cannot reproduce higher frequency variability. The best fit to the composite Sr record was obtained with a sea level variation of 50 m. Given the uncertainty in the estimates of Sr fluxes and rates of recrystallization, we estimate that this value is accurate within a factor of 2.

The presence of large sea level changes caused by glaciation in the Early Cretaceous is inconsistent with interpretations that the Cretaceous climate was too warm to accommodate continental ice sheets (*26*). Although there is some evidence that the Early Cretaceous may have been cooler than the peak warmth of the mid-Cretaceous (*27*), rapid sea level changes persist in the sequence stratigraphic curve throughout the Cretaceous. The validation of rapid changes in the sequence stratigraphic sea level curve for the Early Cretaceous implicates glaciation as a possible explanation for all such rapid sea level changes. An Antarctic ice cap may have persisted despite overall climatic warmth, because high sea surface temperatures enhance vapor transport to the center of Antarctica, where temperatures may remain below freezing (*28*). The presence of polar ice during the Early Cretaceous is supported by observations of ice-rafted deposits (*29*). Matthews and Frohlich (*30*) suggest that orbital variations may control Antarctic ice volume, forcing sea level changes lasting several hundred thousand years with a periodicity of 2 to 4 million years. If this interpretation is correct, then such glacial episodes may be consistent with an overall warm Cretaceous climate, although they may limit the amount of high-latitude warming.

REFERENCES AND NOTES

1. B. Haq, J. Hardenbol, P. Vail, *Science* **23**, 1156 (1987).
2. S. O. Schlanger, in *Mesozoic and Cenozoic Oceans*, K. Hsu, Ed. (American Geophysical Union, Washington DC, 1986), pp. 61–74.
3. A. Hallam, *Phanerozoic Sea-Level Changes* (Columbia Univ. Press, New York, 1992).
4. K. K. Turekian and J. L. Kulp, *Geochim. Cosmochim. Acta* **10**, 245 (1956).
5. S. O. Schlanger, in *Physical and Chemical Weathering in Geochemical Cycles*, A. Lerman and M. Meybeck, Eds. (Kluwer, Boston, MA, 1988), pp. 323–340.
6. E. Gavish and G. Friedman, *J. Sediment. Petrol.* **39**, 980 (1969); W. H. Harris and R. K. Matthews, *Science* **160**, 77 (1968).
7. B. N. Opdyke and B. H. Wilkinson, *Paleoceanography* **3**, 685 (1988).
8. Sites 391C and 534A are located in the Blake-Bahama Basin off the coast of Florida, and site 603B is located approximately 1000 km to the northeast, off the coast of Virginia.
9. Stable isotope measurements of bulk carbonate were made on a VG Optima gas-source mass spectrometer at Princeton University. Precision (1σ) is 0.05 per mil for $\delta^{18}O$ and 0.03 per mil for $\delta^{13}C$.
10. T. J. Bralower, S. Moneci, H. R. Thierstein, *Mar. Micropaleontol.* **14**, 153 (1989).
11. Sr was measured in bulk carbonate and normalized to 100% $CaCO_3$, measured as acid-insoluble residue or by Ca content. Sr and Ca determinations were made in 1.0 N acetic acid dissolutions by atomic adsorption spectroscopy. Reproducibility is better than 1% (coefficient of variation).
12. H. M. Stoll and D. P. Schrag, data not shown.
13. M. R. Palmer and J. M. Edmond, *Earth Planet. Sci. Lett.* **92**, 11 (1989).
14. The smoothed records reduce the maximum amplitude of the Sr increases from 120 to 80%.
15. Bulk carbonate was flushed with 1.0 N ammonium acetate to remove Sr adsorbed on exchange sites. The carbonate residue was then dissolved in 1.0 N acetic acid as in (*13*).
16. P. Baker, J. M. Gieskes, H. Elderfield, *J. Sediment. Petrol.* **52**, 52 (1982); F. M. Richter and D. J. DePaolo, *Earth Planet. Sci. Lett.* **83**, 27 (1987).
17. F. M. Richter and Y. Liang, *Earth Planet. Sci. Lett.* **117**, 553 (1993).
18. A third-order polynomial fit to long-term variations in $\delta^{18}O$ in each record was subtracted from $\delta^{18}O$. These detrended oxygen isotope data are expressed as per mil increases over the minimum value.
19. N. J. Shackleton, M. A. Hall, D. Pate, *Paleoceanography* **8**, 141 (1993).
20. D. P. Schrag, D. J. DePaolo, F. M. Richter, *Geochim. Cosmochim. Acta* **59**, 2265 (1995).
21. D. P. Schrag, D. J. DePaolo, F. M. Richter, *Earth Planet. Sci. Lett.* **111**, 305 (1992).
22. The effect of Ca variability on Sr partitioning is not included in the model, because the riverine-hydrothermal flux is held constant and Ca is not released during aragonite recrystallization. Initial Sr model concentrations are 1650 ppm for aragonite and 500 ppm for calcite.
23. D. Archer and E. Maier-Reimer, *Nature* **367**, 260 (1994); B. N. Opdyke and J. C. G. Walker, *Geology* **20**, 733 (1992).
24. R. K. Matthews and C. Frohlich, *Geology* **15**, 673 (1987). A smaller amount of total recrystallization scales with the total amount of sea level change implied by the model.
25. We obtained the composite sea level curve by averaging all three $\delta^{18}O$ records, inverting the result, and normalizing to a specified magnitude of sea level change.
26. E. J. Barron, W. W. Hay, E. G. Kauffman, *Geology* **12**, 377 (1984); E. J. Barron, *ibid.*, p. 595.
27. L. A. Frakes, J. E. Francis, J. I. Syktus, *Climate Modes of the Phanerozoic* (Cambridge Univ. Press, New York, 1992).
28. M. L. Prentice and R. K. Matthews, *J. Geophys. Res.* **96**, 6811 (1991).
29. L. A. Frakes and J. E. Francis, *Nature* **333**, 547 (1988).
30. R. K. Matthews and C. Frohlich, *J. Geophys. Res.* **96**, 6797 (1991).

31. Supported in part by an Office of Naval Research graduate fellowship to H.M.S. Conversations with F. Richter, M. Monahan, and P. Koch were instrumental in developing this project.

6 February 1996; accepted 19 April 1996

Fine-Scale Doppler Radar Observations of Tornadoes

Joshua Wurman,* Jerry M. Straka,* Erik N. Rasmussen

Observations obtained with a mobile pencil-beam Doppler radar revealed many previously unresolved structures within tornadic storms and tornadoes and helped verify various aspects of conceptual models. Radar data from the parent circulations indicate the existence of spiral reflectivity bands, intense radial wind shear zones, and multiple larger-scale velocity maxima. Tornado structures observed include debris shields, clear axial (eye) regions, multiple reflectivity bands surrounding the center of the eye, and occasional reflectivity protrusions into the eye. Velocity and reflectivity data from tornado-scale circulations show evidence of axial downdrafts.

A widely accepted conceptual model of the flow regions in and around a tornado (Fig. 1) has been developed over the past two decades on the basis of numerous theoretical, numerical, and observational studies (*1*–*6*). The vortex of the tornado is embedded in a swirling, rising outer-flow region (region I), which usually is associated with the parent thunderstorm mesocyclone on a larger scale (radius 5 to 10 km) and with the tornado cyclone on a somewhat smaller scale (radius 1 to 3 km). The flow approximately conserves angular momentum in this region. The core region of the tornado (region II) is thought to be nearly axisymmetric and is characterized by flow that spirals radially inward and upward. This region extends out to about the radius of the maximum tangential winds. The winds in this regime are approximately in cyclostrophic balance (a balance between the horizontal pressure gradient force and the centrifugal force), which helps suppress turbulence and radial flow. Cyclostrophic pressure deficits associated with stronger rotation in the lower levels than in the upper levels can accelerate the movement of air downward along the central axis. The corner-flow region in the tornado (region III) is characterized by intense, frictionally induced, radial inflow that must turn abruptly upward, owing to vertical pressure gradients, before reaching the axis. In the surface boundary layer region (region IV), friction produced by the lower boundary (the Earth's surface) retards the rotating flow. This disrupts the cyclostrophic wind balance, and flow accelerates radially inward toward the axis of rotation. Finally, the convective plume region (region V) is where angular momentum concentrated in the lower levels of the tornado circulation is transported outward by divergence or turbulence. Up to this time, observations to verify this conceptual model of a tornado have been unavailable.

In this report, we present close-range (2 to 6 km), fine-scale resolution volume (50 to 130 m), 3-cm band radar reflectivity and pulsed Doppler weather radar observations of a violent tornado that were obtained as part of the Verification of the Origins of Rotation in Tornadoes Experiment (VORTEX) field program (*7*). Earlier pulsed Doppler radar observations of tornadoes have been at more distant ranges (12 to 60 km), resulting in wider resolution volume

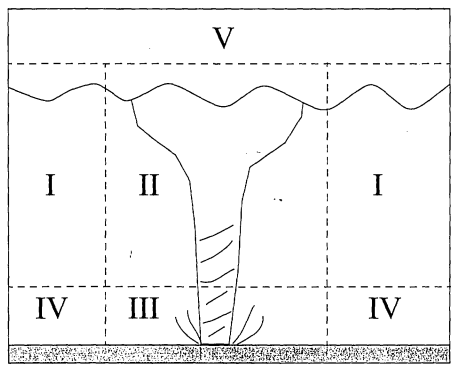

Fig. 1. Conceptual model of the flow regimes associated with a tornado: region I, outer flow; region II, core; region III, corner; region IV, surface boundary layer; region V, convective plume (*1*–*6*).

J. Wurman, School of Meteorology, University of Oklahoma, 100 East Boyd Street, Norman, OK 73019, USA.
J. M. Straka, School of Meteorology, Center for Analysis and Prediction of Storms and Cooperative Institute for Mesoscale Meteorological Studies, University of Oklahoma, 100 East Boyd Street, Norman, OK 73019, USA.
E. N. Rasmussen, National Severe Storms Laboratory, 1313 Halley Circle, Norman, OK 73069, USA.

*These authors contributed equally to this work.